Automatic Parameter Estimation for Graph-Cut Chan-Vese for Fluorescence Image Binarization

Ryan Naidoo, Jules-Raymond Tapamo

Abstract

Motivation The detailed analytical studies of microscopic organisms and such have played a vital role in a host of fields ranging from the simple curiosity of what goes on at the mirco-level to studying the behaviour of cancerous cells. Fluorescence images are generated by the thousands to study these phenomena. The rate at which we're able to gather data outweighs the rate at which we're able to accurate study it. The key to efficient and effective study lies heavily on the ability to bring into focus what is needful and discard everything else. In the study of fluorescence images, it is absolutely critical that the object be segmented accuratetly and quickly. The optical challenges present in fluorescence images make it a very unique class of image data, as such, other segmentation parameters settings cannot be readily applied to it. One must start at the ground level to find the optimal parameters for accurate segmentation; which is tedious and an ineffective use of time. There is also a large variance in the types of images within the set of fluorescence images and hard-coded parameters are quick to hit a brick wall, and once again it is back to the drawing board for searching out the correct parameters for segmentation. **Purpose** The purpose of this study is too investigate the properties of fluorescence images and leverage that understanding to develop a technique that is able to autoatically produce image-specific accurate parameter settings for segmentation of the object of interest. **Proposition** In this paper, we present a novel parameter estimation technique for the graph cut implementation of the Chan-Vese approximation of the Mumford-Shah functional for image segmentation. **Results** The effectiveness of the technique is demonstrated through a set of experiments with real images. These images are chosen such that the set has broad coverage wit the type of images that are commonly obtained in fluorescence imaging. We pit our approach against two other common paramter settings. Our approach proves superior and highly robust for a large range of image types. (Give actual percentages here.)

Keywords

Image segmentation, graph cuts, fluorescence, active-contours, Chan-Vese.

I. Introduction

Lay the foundation to present the problem. Amount of images. Problems with the images. The type of solutions available that miss solving the problem. **Present the problem. What solution do we seek. Scope of the paper. Other tried approaches. What are their weaknesses? What did they sacrifice to get that scheme or result. What schemes will we be competing with. Organisation.**

II. Chan-Vese Formulation of the Mumford-Shah Energy Functional

The Mumford-Shah evolution energy functional is a segmentation model to be minimised over an approximation image u of the input image u_0. The level set representation of the Mumford-Shah energy function is

$$\begin{aligned} F(c_1, c_2, \phi) = \mu \int_\Omega \delta(\phi(x,y))|\nabla\phi(x,y)|dxdy \\ + \nu \int_\Omega H(\phi(x,y))dxdy \\ + \lambda_1 \int_\Omega |u(x,y) - c_1|^2 H(\phi(x,y))dxdy \\ + \lambda_2 \int_\Omega |u(x,y) - c_2|^2 (1 - H(\phi(x,y)))dxdy, \end{aligned} \tag{1}$$

where λ_1, λ_2, μ, and ν are fixed parameters such that $\lambda_1, \lambda_2 > 0$ and $\mu, \nu \geq 0$. $u(x,y)$ is the image, $H(\cdot)$ is the Heaviside step function, $\delta(\cdot)$ is the Dirac delta function, Φ is an open unbounded subset of $\Re^2$ and $\phi : \Omega \to \mathbb{R}$ is the level set function, such that:

$$\begin{aligned} \omega &= \{(x,y) \in \Omega | \Phi(x_p) > 0\} \\ \bar{\omega} &= \{(x,y) \in \Omega | \Phi(x_p) < 0\} \\ C = \partial\omega &= \{(x,y) \in \Omega | \Phi(x_p) = 0\}, \end{aligned} \tag{2}$$

c_1 and c_2 are the arithmetic means of the intensities in the regions of u defined by the masks $H(\phi(x,y)$ and $1 - H(\phi(x,y)$ respectively. The piece-wise smooth approximation of the image is then

$$u(x,y) = c_1 H(\phi(x,y)) + c_2(1 - H(\phi(x,y))). \tag{3}$$

A. Discretising the Mumford-Shah Functional

With the exception of the second term in Equation (1), the remaining terms can be represented discretely very easily. For each pixel $p \in \Omega$, let x_p be a binary variable such that

$$x_p = \begin{cases} 0 & \phi(p) \leq 0 \\ 1 & \phi(p) > 0 \end{cases} \tag{4}$$

The means can now be calculated using

$$c_1 = \frac{\sum_p u(x,y) x_p}{\sum_p x_p}, \tag{5}$$

$$c_2 = \frac{\sum_p u(x,y)(1 - x_p)}{\sum_p (1 - x_p)}. \tag{6}$$

For simplification, set $\nu = 0$. Kolmogorov and Boykov in [] used the Cauchy-Crofton thereom to approximate the length of a contour C by counting the number of intersections with the line L. By using this approximation, it can be shown that the Euclidean contour length can be expressed as

$$\|C\|_E = \sum_{p,q \in e_k} w_k (x_p(1 - x_q) + x_q(1 - x_p)). \tag{7}$$

The fully discrete form of Equation (1) is

$$\begin{aligned} F(x_1,\ldots,x_n) = \mu \sum_{p,q\in e_k} w_k(x_p(1-x_q)+x_q(1-x_p)) \\ + \lambda_1 \sum_p |u(x,y)-c_1|^2 x_p \\ + \lambda_2 \sum_p |u(x,y)-c_2|^2 (1-x_p) \end{aligned} \tag{8}$$

III. Graph-Cut Model for Chan-Vese Segmentation

Graph Cuts are a well known optimisation problem in Combinatronics. Due to the duality known as the Max-Flow Min-Cut Thereom, there are several fast algorithms to find the mincut. Typically, it's easier to solve the the Max-Flow problem and bulk of the optimised algorithms are designed on Max-flow algorithms. Graph Cuts were unsuccesfully introduce into Computer Vision by Greig *et al.* [] and was later popularised by Kolmogorov [].

A graph $G = (V, E)$ is a set of vertices/nodes V, and a set of directed edges E with positive weights/capacities that connect these vertices. We let uv be a directed edge going from u to v. The weight of the edge is denoted by $c(u, v)$. In the 2-label graph cut, there are two more vertices that don't correspond to any pixels. These are the source s and the sink t. All other nodes are directly connected to both the source and the sink. Therefore, a cut on G is a partioning of V into two disjoint connected sets (V_s, V_t) such that $s \in V_s$ and $t \in V_t$. The cost of the cut is calculated as

$$c(V_s, V_t) = \sum_{i\in V_s, j\in V_t} c(i, j). \tag{9}$$

Graph cuts are used to minimise energies of the form

$$\arg\min_{x\in\{0,1\}^m} E(x) = \sum_i E^i(x_i) + \sum_{i<j} E^{i,j}(x_i, x_j). \tag{10}$$

For an energy to be graph-representable, the pairwise interaction potentials must be submodular [], i.e. it must adhere to the following constraint.

$$E^{i,j}(0,0) + E^{i,j}(1,1) \leq E^{i,j}(0,1) + E^{i,j}(1,0),\ \forall i < j. \tag{11}$$

It has been shown in [] that Equation (8) is submodular and hence the optimal solution can be found via graph cuts. The data and regularisation energy respectively in Equation (10) is

$$E^i(x_i) = \lambda_1 |u(x,y)-c_1|^2 x_i + \lambda_2 |u(x,y)-c_2|^2 (1-x_i) \tag{12}$$

$$E^{i,j}(x_i, x_j) = (x_i + x_j - 2x_i x_j) w_{ij} \tag{13}$$

IV. Chan-Vese Parameter Estimation for Graph-Cuts

In this section we introduce the proposed method for Chan-Vese parameter estimation for graph-cuts. Previous parameter estimation schemes focussed on a certain genre of images or image characteristics, and these resulted in a set of hard-coded parameter settings. These hard-coded parameters are not very useful in producing consistent reults in the greater applications of image segmentation even within the fields for which they were optimised.

We devise a novel weighting scheme for the graph and propose a general parameter estimation technique in which the parameters adapt themselves to the image. We achieve this not by focusing on the parameters, but rather the relationship between the parameters. We then isolate these relationships in proxy relational parameters which we then tune for fluorescence images.

A. Proposed Technique

We first explain the method used to weight the graph. We begin by normalising the data and smoothing connections. We use the Euclidean distance to weighting of the edges connecting adjacent nodes, i.e. diagonally adjacent node in the 8-connected graph would be scaled by $\frac{1}{\sqrt{2}}$, etc.

The image pixel values are also normalised i.e. $p \in [0, 1]$, where p is the pixel value of the i-th pixel in the image. The edge connecting the source to the node which corresponds to pixel i is given by $E^i(0)|_{i=p} = \lambda_0|p - c_0|^2$. This is how far away the pixel is from the average foreground/object pixel intensity c_0. Similarly, the weight of the connection from the node to the sink is given by $E^i(1)|_{i=p} = \lambda_1|p - c_1|^2$, i.e. how far away the pixel is from the average background pixel intensity c_1.

Whether a node is connected to the source or the sink after segmentation depends on its connections which are wighted by the previously defined energy functions. It behooves use to study then, the relationship between the energy functions. We see that there are two tunable parameters namely λ_0 and λ_1. It is the relationship between these two parameter that heavily influence the output. We simplify and explicitely formalise the relationship between and set

$$\lambda_0 = \alpha\lambda_1. \tag{14}$$

Forcing this relationship make further analysis simpler and more intuitive. An immediate constraint is $\alpha > 0$, since we require all data conenctions to be positive, i.e $E^i(0), E^i(1) \geq 0$.

We will now analyse the flow through a single node in the 8-connected graph, we use Figure 1 to facilitate our explanation. Two nodes are maximally connected if their corresponding pixel values are the same, i.e. there is no difference between them. Let this value be μ. Hence, the maximum possible flow into or out of a node to its neighbours is

$$f_{max} = 4\mu + 4\frac{\mu}{\sqrt{2}} = \mu\left(2\sqrt{2} + 4\right). \tag{15}$$

We know that for a node p to belong to the source set, i.e. $p \in S$, the incoming flow from the source must completely saturate all outlets. This can be expressed as

$$E^i(0) > E^i(1) + \mu\left(2\sqrt{2} + 4\right). \tag{16}$$

Similarly, to guarantee the node will be in the sink set, $p \in T$, we have

$$E^i(1) > E^i(0) + \mu\left(2\sqrt{2} + 4\right). \tag{17}$$

To aid in understanding the energies, we use Figure 2.

For quadratic energies with $0 < c_0 < c_1 < 1$, there is a point, between c_0 and c_1, where the incoming flow from the source completely saturates the sink with no excess remaining. This point, where the energies are equal,

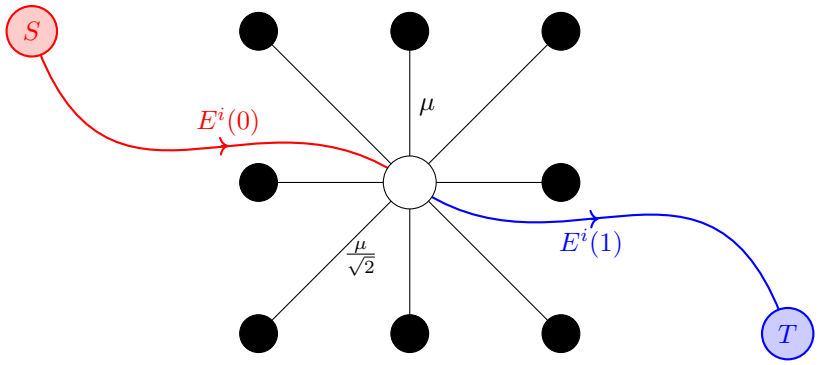

Fig. 1. Fully connected single node.

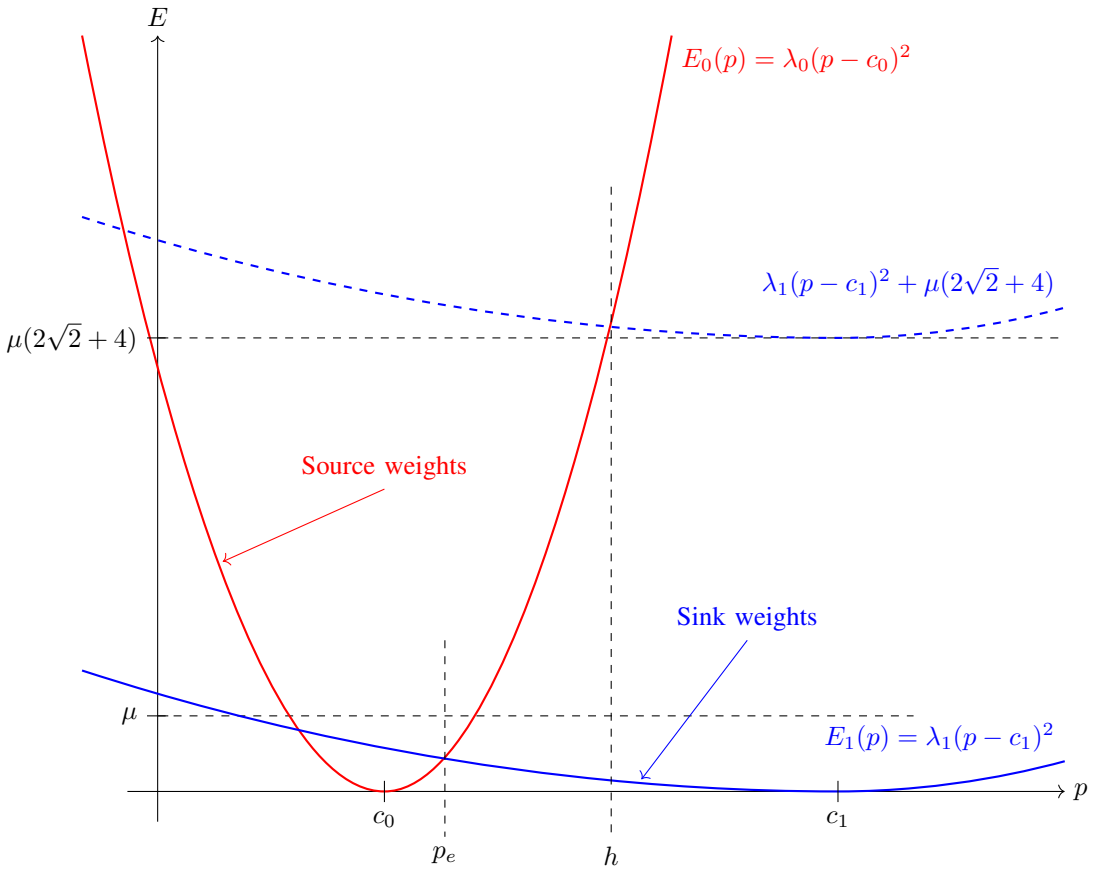

Fig. 2. Data energy functions plot.

we call p_e, i.e. $E_0(p_e) = E_1(p_e)$. Taking into account the relation in Equation (14), this point of zero net flow is found to be

$$p_e = c_0 + \frac{c_1 - c_0}{\sqrt{\alpha} + 1} \tag{18}$$

The point where the energies are equal, p_e, is shown in Figure 2.

We now shift our focus on the relationship between p_e and α. We see that α is the only tuneable parameter. From this inverse relationship we note three major points. These are

$$\text{if } \alpha = 1, p_e = c_0 + \frac{c_1 - c_0}{1 + \sqrt{1}} = \frac{c_0 + c_1}{2} \qquad \text{(midpoint between } c_0 \text{ and } c_1\text{)}$$

$$\lim_{\alpha \to \infty} p_e = c_0 \qquad \text{(maximum } \alpha \text{ yields lower-bound on } p_e\text{)}$$

$$\lim_{\alpha \to 0} p_e = c_1 \qquad \text{(minimum } \alpha \text{ yields upper-bound on } p_e\text{)}$$

This is relationship is shown graphically in Figure 3.

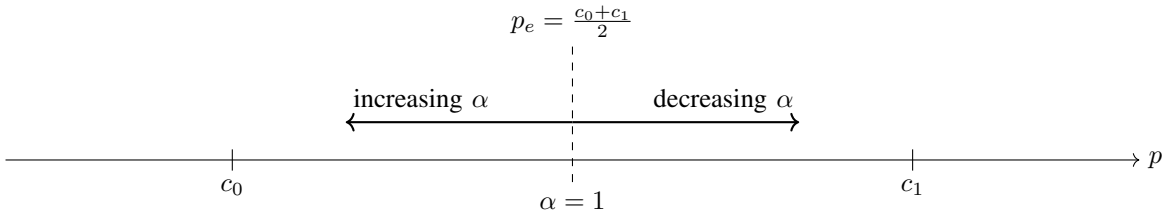

Fig. 3. Relationship between α and p_e.

If we can make a good estimation for p_e, c_0 and c_1 for the segmentated image, then it can be shown that the corresponding α can be calculated as

$$\alpha = \left(\frac{c_1 - c_0}{p_e - c_0} - 1 \right)^2 \tag{19}$$

When we calculated the intersection between the energies p_e, we ignored the other point that was out of the range $[c_0, c_1]$.Let this point be p_{e^*}. If this point is positive and $0 < p_{e^*} < c_0$ then we must ensure that at no point within this range must the source flow saturate all outgoing edges. This forces a limit on how low μ can be. This is only of significant concern when $\alpha > 1$. We only need to concern ourselves with the point $p = 0$ as this is the point where the difference $E^i(0) - E^i(1)$ is the largest. Taking into account the relation in Equation (14), the lower-bound on μ can be shown to be

$$\mu > \frac{\lambda_1(\alpha c_0^2 - c_1^2)}{\left(2\sqrt{2} + 4\right)} \tag{20}$$

From Equation (16) we can see that there is a point beyond which all nodes which correspond to pixel value higher than that point will be saturated and have excess flow; this means that they will be in the source set. We will call this point the *saturation point* and denote it by h. This is shown in Figure 2. This point can be determined using

$$h = \frac{(\alpha c_0 - c_1) + \sqrt{\alpha(c_0 - c_1)^2 + \frac{\mu(2\sqrt{2}+4)}{\lambda_1}(\alpha - 1)}}{\alpha - 1} \tag{21}$$

This point is marked off in Figure 2.

Therefore, given good approximations for c_0, c_1, α, h and μ, we can calculate the appropriate value for λ_1. This can be shown to be

$$\lambda_1 = \frac{\mu(2\sqrt{2} + 4)}{\alpha(h - c_0)^2 - (h - c_1)^2} \tag{22}$$

The parameter estimation is based on the assumption that sufficiently good approximations for c_0, c_1, p_e and h can be obtained. By sufficiently good we are referring to the closeness to the values these parameters would be for

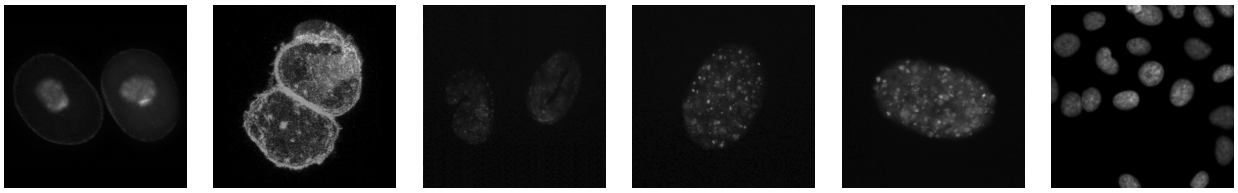

(a) Image 1 (b) Image 2 (c) Image 3 (d) Image 4 (e) Image 5 (f) Image 6

Fig. 4. Images from tuning set.

an ideal segmentation. From these approximations, we calculate α using Equation (19). The parameters μ and λ_1 are not separable, therefore we choose to set μ. We can then calculate λ_1 using Equation (22). Finally λ_0 can be calculated using Equation (14). In the next section we discuss how we make the guess for good approximations for the required parameters.

B. Tuning the Proxy Parameters

The properties of the images obtained in fluorescence microscopy imaging can be used to guide the parameter estimation process. We focus specifically on black background fluorescent images. Due to the fact that the predominant form of noise in the imaging system in Poisson distributed, we can further assume that the darker the background, the less noise that is present therein. The Poisson process also tells us that brighter regions exhibit a greater intensity variation due to the sampling process. Therefore, the curve for $E^i(1)$ is less convex than $E^i(0)$ as in Figure 2 and, resultantly, the value for p_e, in Figure 3, is shifted to the left. This places a new lower-bound on α for fluorescence images

$$\alpha \geq 1. \tag{23}$$

The tuning process we used is as follows: We manually segmented the fluorescent images in Figure 4. The segmentation results that were closest to the groundtruth were chosen and the corresponding proxy parameters were calculated for each image. The final setting for the proxy parameter was taken as the average value for each proxy parameter from all images.

Since the curves energy functions, $E^i(0)$ and $E^i(1)$, can be tuned relative to a fixed value for μ, which this would not impact significantly on the range of possible solution sets, we set $\mu = 1$ in all our manual parameter tuning. We use a stopping criterion of $\epsilon = 1 \times 10^{-3}$. We compared the effect of using Otsu binarization, K-means ($k = 2$) and Expectation-Maximisation for Gaussian Mixture Modelling (EMGMM) with ($k = 2$) for generating the initial means, $c0$ and c_1. The values used for $\alpha \in [1, 10, 20, 30, 40, 45, 50]$ and the values used for $\lambda_1 \in [50, 100, 150, 200, 400, 800]$. The remaining parameters were calculated from μ, α and λ_1.

As final results we take the means of the final segmentation for the background and foreground regions. An acceptable solution was one that achieved at least 70% of the final means from the ground truth for each region. From the acceptable results, we calculate the values for p_e, Equation (18), and h, Equation (21). The means for each image can vary greatly. To put the values of p_e and h into a relative perspective, they are shown as a fraction of the distance between c_0 and c_1. Let $k_p \in (0, 1)$ be the fraction of the distance $p_e - c_0$ and $c_1 - c_0$ as illustrated

in Figure 5. Let $k_h \in (k_h, 1)$ be the fraction of the distance $h - c_0$ and $c_1 - c_0$ as illustrated in Figure 6, we have $0 < k_p < k_h$.

Fig. 5. p_e as a fraction of the distance between c_0 and c_1.

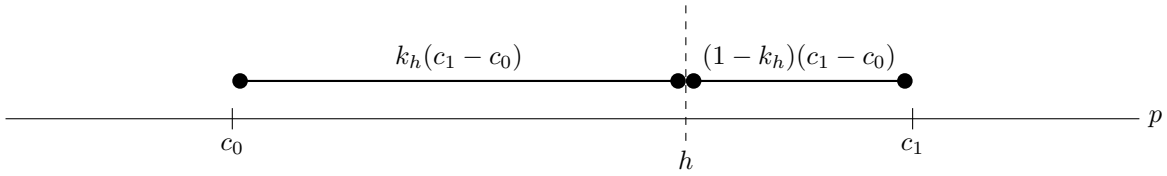

Fig. 6. h as a fraction of the distance between c_0 and c_1.

Upon comparing the initial means and final means for the acceptable segmentation results, it was noted the the values of the initial means are larger. This is due to over-segmentation produced by Otsu, K-means and EMGMM clustering. A naïve approach to shifting the initial means closer to the final means is to dilate the initial mask. This pushes the boundaries of the contour for the object to accept the lower intensity neighbouring pixels, as well as remove these relatively higher values from the background mask. If we are able to make a better guess to the initial means, then the fewer iterations are needed to converge within the stopping criterion.

To determine the optimal dilation size, we compare the difference of the mean values for each image, for the acceptable segmentation results only. We use an elliptical element for dilation and the size of the dilation ranged from $r \in [1, 2, 3, 5, 7, 9]$. A dilation size of 3 for a elliptical dilation element results in mean values that are closest to the average final means.

When defining the values for p_e and h implicitly and k_p and k_h respectively, we find the updated equation for determining α is simplified to

$$\alpha = \left(\frac{1 - k_p}{k_p}\right)^2 \tag{24}$$

The weighting parameter λ_1 can be calcualted as

$$\lambda_1 = \frac{\mu\left(2\sqrt{2} + 4\right)}{(c_1 - c_0)^2\left(\left(\frac{1-2k_p}{k_p^2}\right)k_h^2 + 2k_h - 1\right)} \tag{25}$$

For determining α we found the average of all k_p for all acceptable segmentations. This is calculated to be

$$k_p = 0.154494.$$

From this we can calculate the value for α immediately using Equation (24). This turns out to be

$$\alpha = 29.9509. \tag{26}$$

Similarly, to determine h we find the average of all k_h for all acceptable segmentations. This is calculated to be

$$k_h = 0.412737.$$

An appropriate value for λ_1 depends on c_0 and c_1, as can be seen in Equation (25), which can only be determined after the inital means are generated.

C. Parameter Estimation Process

We now present the final parameter estimation process. The parameters whose values are fixed are

1) $\mu = 1$
2) $k_p = 0.154494$
3) $k_h = 0.412737$
4) $\alpha = 29.9509$

We first segment the image to determine the initial c_0 and c_1. We can then calculate λ_1 using Equation (25). Finally, we can calculate λ_0 using Equation (14). The remaining parameter is the stopping criterion ϵ which we set to 1×10^{-3}.

V. Experimental Results

We compare our results to two previously published parameter settings. Their results showed excellent segmentation output on synthetic images and mammography images with very high robustness against noise. They do not specify the noise type. Their parameter setting was based on a time-lapse series of fluorescence images. Their scheme is a hybrid of algorithms designed to segment whole fluorescent cells; however, we use the parameter setting they have presented for segmentation only. Their parameter setting was obtained by minimising the Jaccard coefficient over the time-lapse series.

To generate the initial means we used the EMGMM with $k = 2$ which was followed by an elliptical dilation of size 3. The results of all segmentation scheme are shown from Figure 7 to Figure 31.

In Table I, which compares the segmentation efficiency of each method, we differentiate between methods on the same image as follows:

[imageno]-[method],

where *imageno* goes from 1 to 25 and *method* is defined as follows:

- **n** - using parameter setting presented by El-Zehiry *et. al*
- **m** - using parameter setting presented by Masaka *et. al*
- **d** - Proposed method with parameters estimated from an initial EMGMM segmentation with $k = 2$ and an elliptical dilation of $3px$.

In Table I we compare the accuracy and MCC of each segmented result for each scheme. Accuracy is the fraction of the pixels that are correctly classified from among all pixels. MCC is the *Matthews Correlation Coefficient* and is more accurate measure of accuracy when comparing classes whose sizes differ greatly.

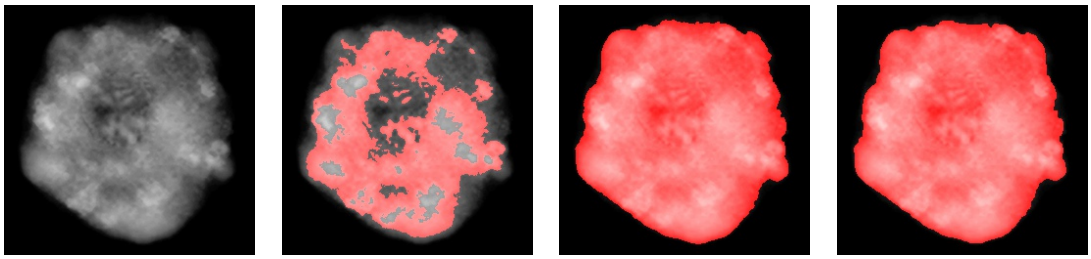

(a) Original. (b) El-Zehiry *et al*. (c) Masaka *et al*. (d) Proposed. $\lambda_1 = 8.17148$.

Fig. 7. Image 1 from test set segmentation results.

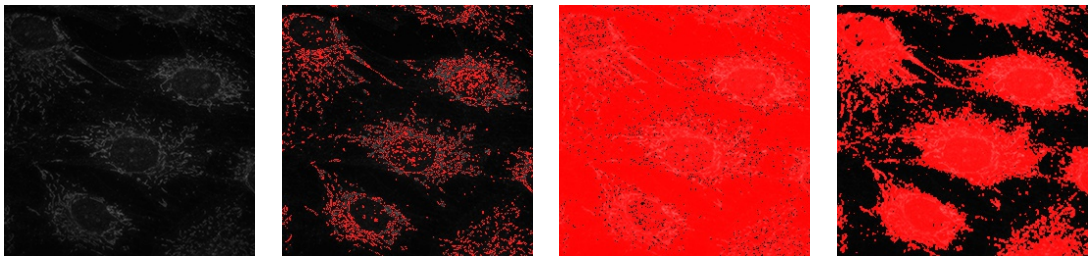

(a) Original. (b) El-Zehiry *et al*. (c) Masaka *et al*. (d) Proposed. $\lambda_1 = 606.199$.

Fig. 8. Image 2 from test set segmentation results.

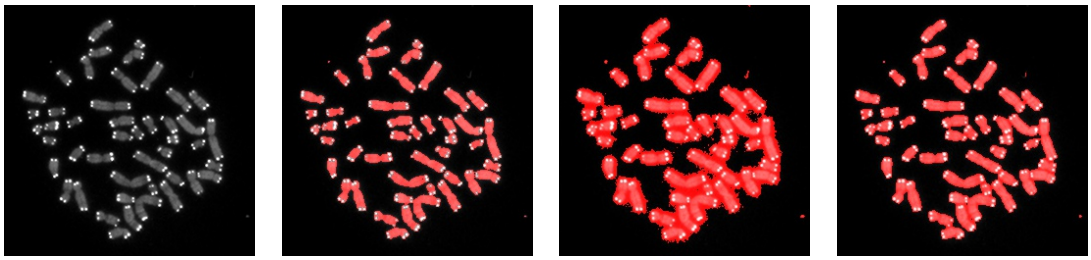

(a) Original. (b) El-Zehiry *et al*. (c) Masaka *et al*. (d) Proposed. $\lambda_1 = 32.3237$.

Fig. 9. Image 3 from test set segmentation results.

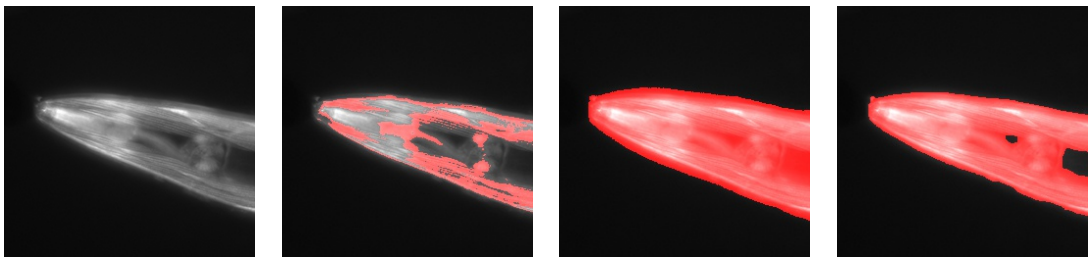

(a) Original. (b) El-Zehiry *et al*. (c) Masaka *et al*. (d) Proposed. $\lambda_1 = 11.5385$.

Fig. 10. Image 4 from test set segmentation results.

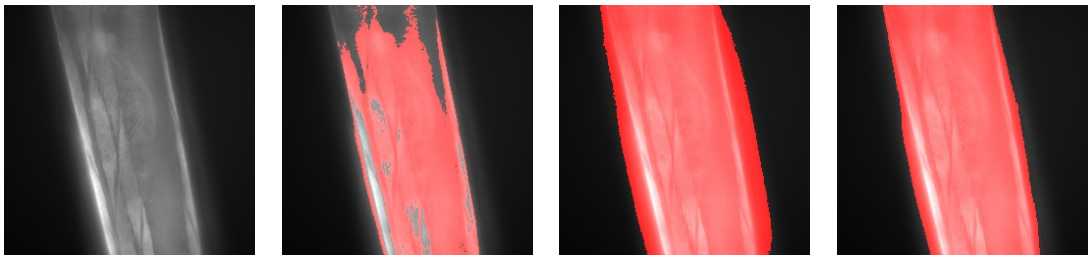

(a) Original. (b) El-Zehiry *et al*. (c) Masaka *et al*. (d) Proposed. $\lambda_1 = 11.2011$.

Fig. 11. Image 5 from test set segmentation results.

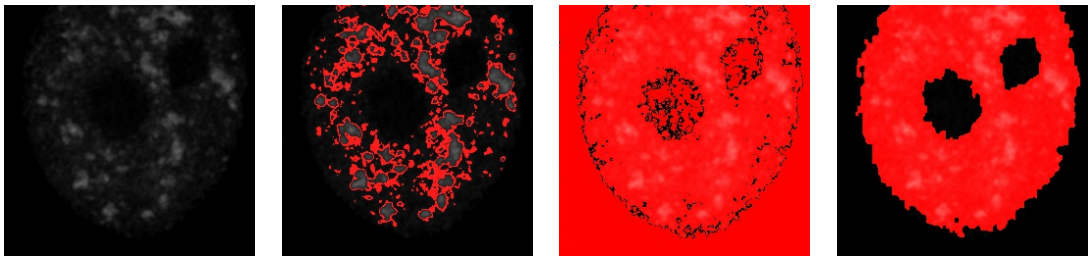

(a) Original. (b) El-Zehiry *et al*. (c) Masaka *et al*. (d) Proposed. $\lambda_1 = 161.108$.

Fig. 12. Image 6 from test set segmentation results.

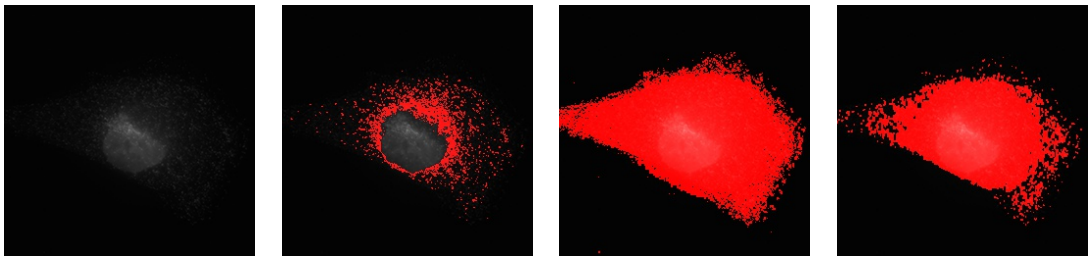

(a) Original. (b) El-Zehiry *et al*. (c) Masaka *et al*. (d) Proposed. $\lambda_1 = 331.532$.

Fig. 13. Image 7 from test set segmentation results.

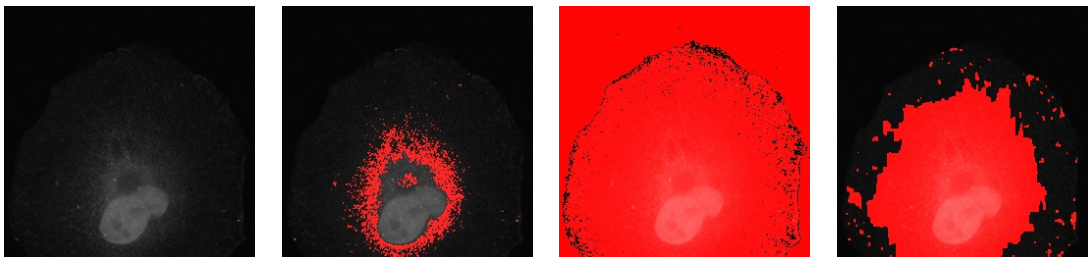

(a) Original. (b) El-Zehiry *et al*. (c) Masaka *et al*. (d) Proposed. $\lambda_1 = 73.2113$.

Fig. 14. Image 8 from test set segmentation results.

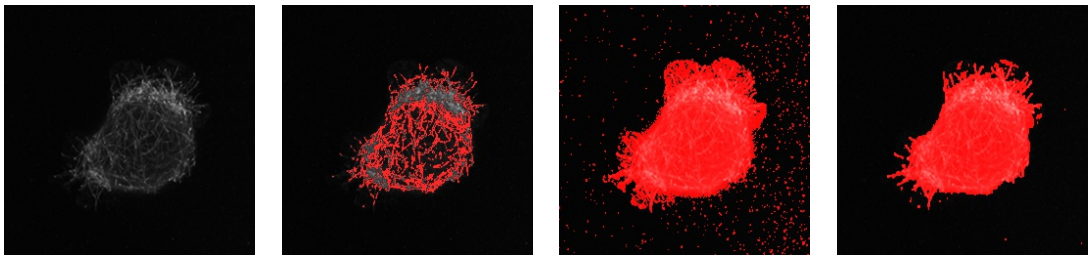

(a) Original. (b) El-Zehiry *et al*. (c) Masaka *et al*. (d) Proposed. $\lambda_1 = 146.629$.

Fig. 15. Image 9 from test set segmentation results.

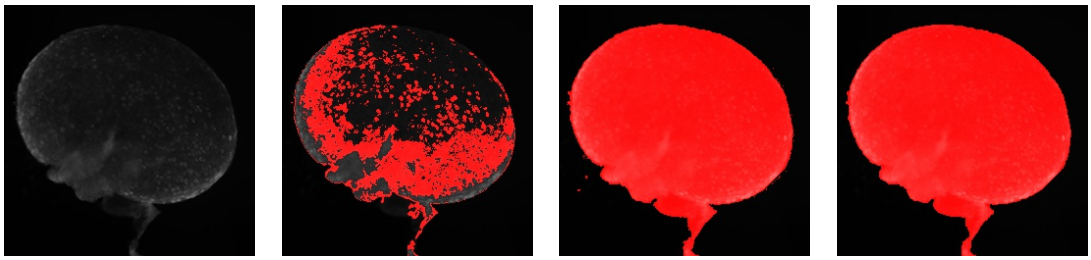

(a) Original. (b) El-Zehiry *et al*. (c) Masaka *et al*. (d) Proposed. $\lambda_1 = 165.378$.

Fig. 16. Image 10 from test set segmentation results.

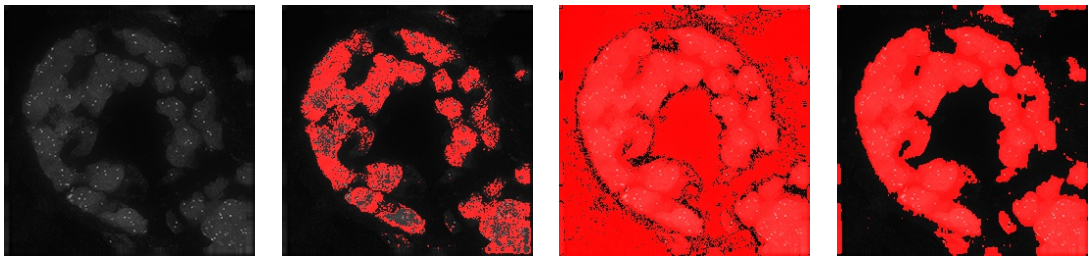

(a) Original. (b) El-Zehiry *et al*. (c) Masaka *et al*. (d) Proposed. $\lambda_1 = 154.458$.

Fig. 17. Image 11 from test set segmentation results.

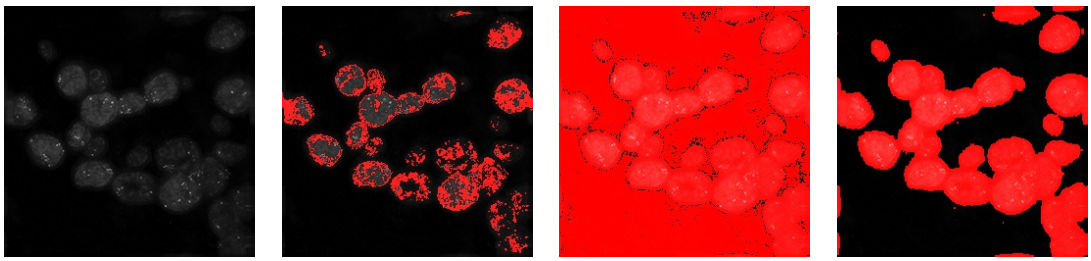

(a) Original. (b) El-Zehiry *et al*. (c) Masaka *et al*. (d) Proposed. $\lambda_1 = 160.407$.

Fig. 18. Image 12 from test set segmentation results.

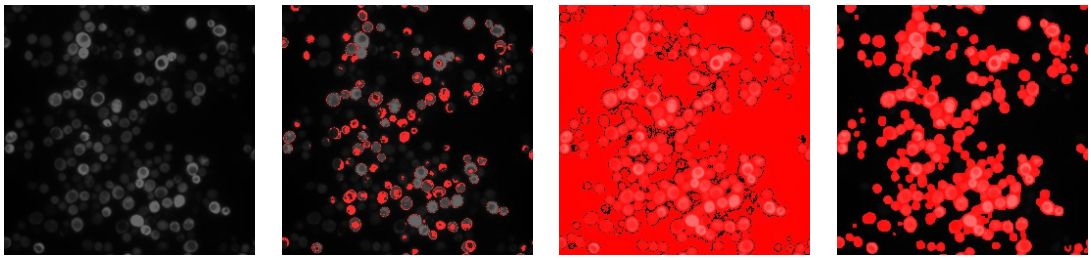

(a) Original. (b) El-Zehiry *et al*. (c) Masaka *et al*. (d) Proposed. $\lambda_1 = 129.64$.

Fig. 19. Image 13 from test set segmentation results.

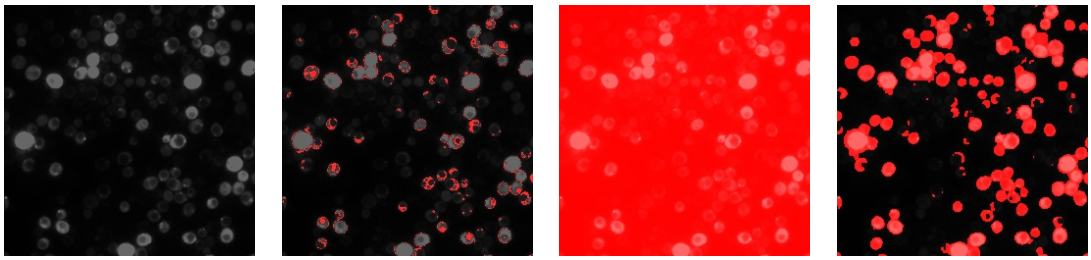

(a) Original. (b) El-Zehiry *et al*. (c) Masaka *et al*. (d) Proposed. $\lambda_1 = 84.6065$.

Fig. 20. Image 14 from test set segmentation results.

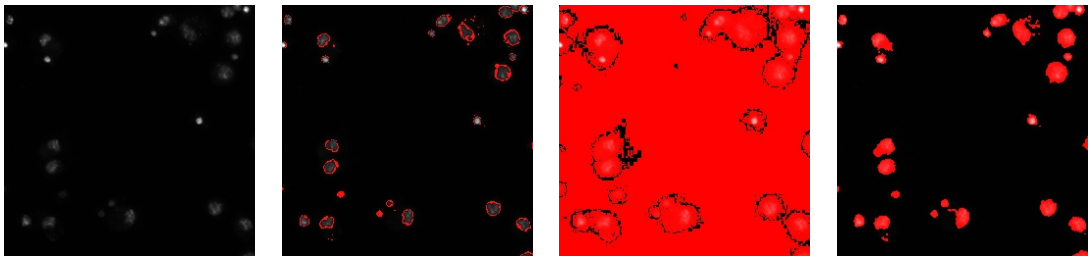

(a) Original. (b) El-Zehiry *et al*. (c) Masaka *et al*. (d) Proposed. $\lambda_1 = 860.426$.

Fig. 21. Image 15 from test set segmentation results.

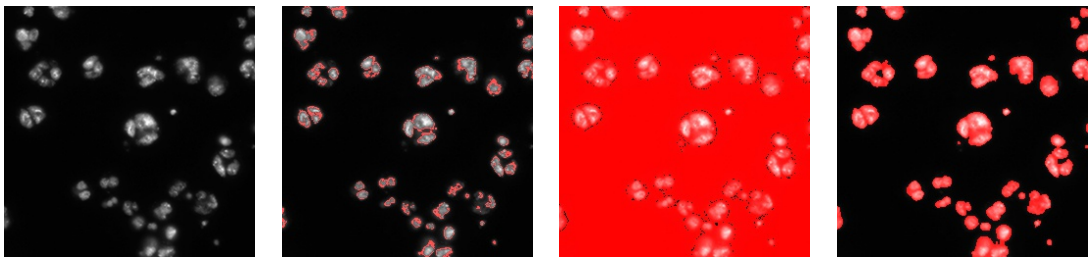

(a) Original. (b) El-Zehiry *et al*. (c) Masaka *et al*. (d) Proposed. $\lambda_1 = 37.6071$.

Fig. 22. Image 16 from test set segmentation results.

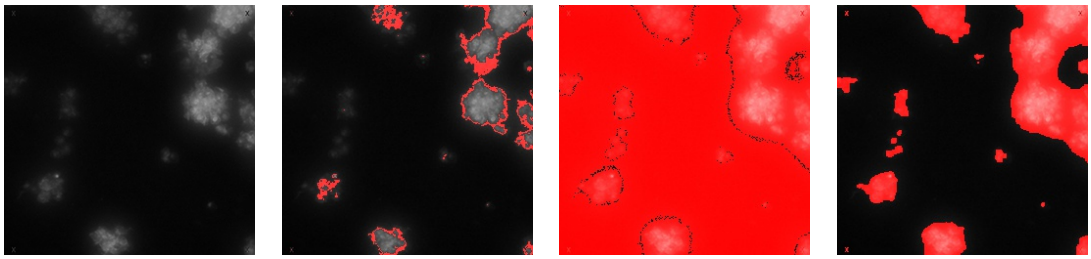

(a) Original. (b) El-Zehiry *et al*. (c) Masaka *et al*. (d) Proposed. $\lambda_1 = 43.33$.

Fig. 23. Image 17 from test set segmentation results.

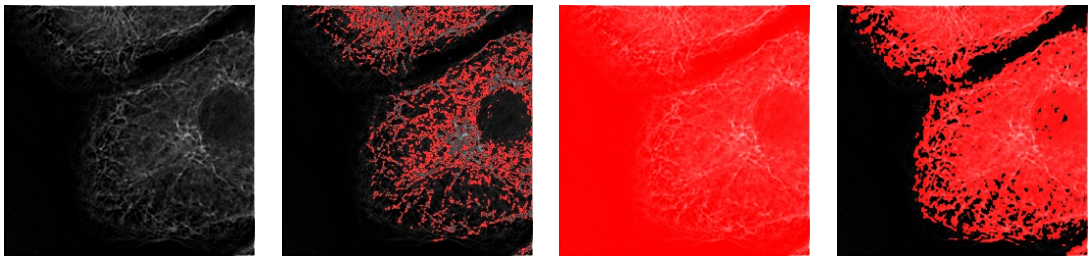

(a) Original. (b) El-Zehiry *et al*. (c) Masaka *et al*. (d) Proposed. $\lambda_1 = 85.0788$.

Fig. 24. Image 18 from test set segmentation results.

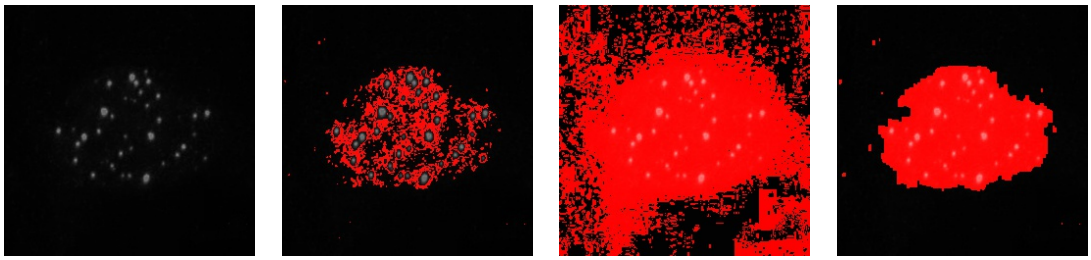

(a) Original. (b) El-Zehiry *et al*. (c) Masaka *et al*. (d) Proposed. $\lambda_1 = 309.766$.

Fig. 25. Image 19 from test set segmentation results.

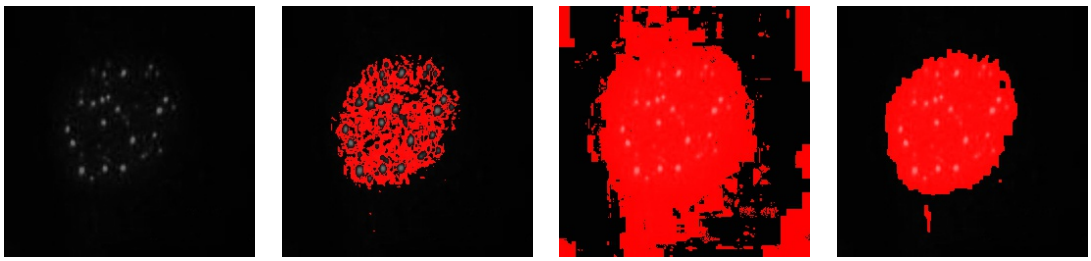

(a) Original. (b) El-Zehiry *et al*. (c) Masaka *et al*. (d) Proposed. $\lambda_1 = 359.465$.

Fig. 26. Image 20 from test set segmentation results.

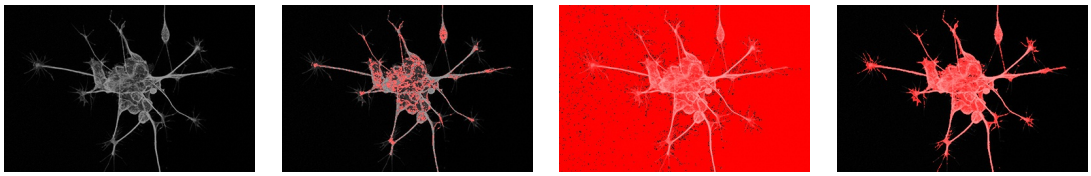

(a) Original. (b) El-Zehiry *et al*. (c) Masaka *et al*. (d) Proposed. $\lambda_1 = 359.465$.

Fig. 27. Image 21 from test set segmentation results.

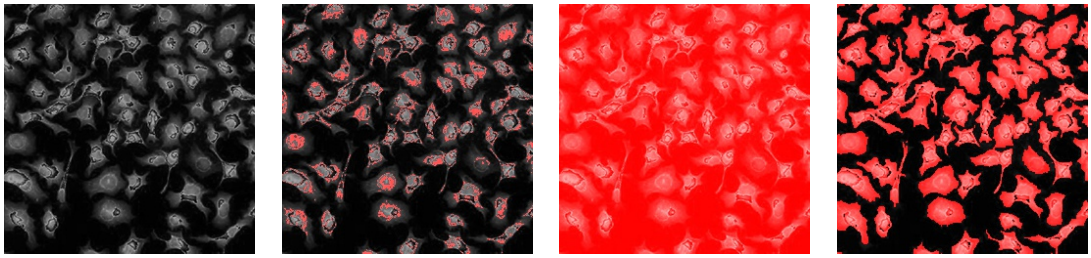

(a) Original. (b) El-Zehiry *et al*. (c) Masaka *et al*. (d) Proposed. $\lambda_1 = 38.837$.

Fig. 28. Image 22 from test set segmentation results.

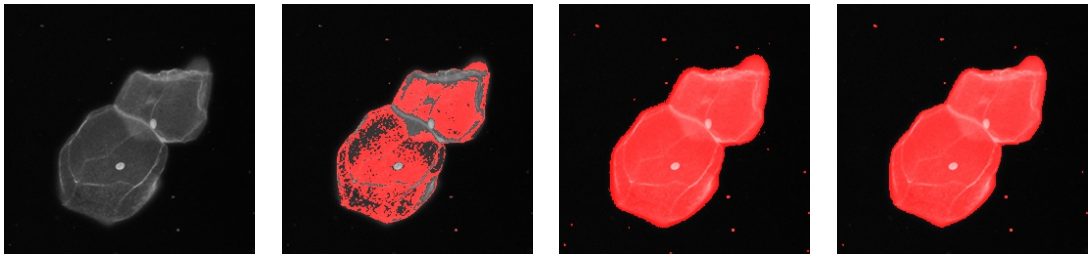

(a) Original. (b) El-Zehiry *et al*. (c) Masaka *et al*. (d) Proposed. $\lambda_1 = 34.8846$.

Fig. 29. Image 23 from test set segmentation results.

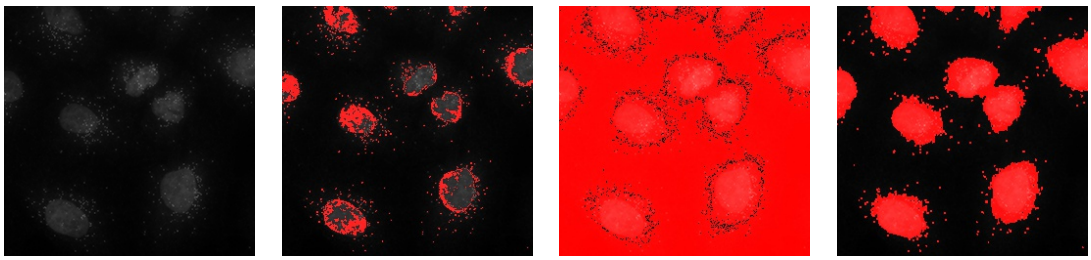

(a) Original. (b) El-Zehiry *et al*. (c) Masaka *et al*. (d) Proposed. $\lambda_1 = 249.515$.

Fig. 30. Image 24 from test set segmentation results.

TABLE I: Segmentation Efficiency.

Image	TP	TN	FP	FN	Precision	Recall	Accuracy	MCC
1-n	24954	25516	0	15066	1.000000	0.623538	0.770111	0.626140
1-m	37875	25506	10	2145	0.999736	0.946402	0.967117	0.934010
1-d	37364	25513	3	2656	0.999920	0.933633	0.959427	0.919468
2-n	5561	43411	179	16385	0.968815	0.253395	0.747253	0.416180
2-m	21864	120	43470	82	0.334650	0.996264	0.335449	-0.008374
2-d	21867	34669	8921	79	0.710244	0.996400	0.862671	0.748686
3-n	9113	55407	24	992	0.997373	0.901831	0.984497	0.939774
3-m	10105	47657	7774	0	0.565188	1.000000	0.881378	0.697081
3-d	10105	53847	1584	0	0.864488	1.000000	0.975830	0.916397
4-n	10654	49844	99	4939	0.990793	0.683255	0.923126	0.783314
4-m	15593	46825	3118	0	0.833360	1.000000	0.952423	0.883930
4-d	14920	48593	1350	673	0.917025	0.956840	0.969131	0.916491
5-n	21195	38591	2276	3474	0.903029	0.859175	0.912262	0.811918
5-m	24669	31160	9707	0	0.717623	1.000000	0.851883	0.739708
5-d	24669	35427	5440	0	0.819323	1.000000	0.916992	0.842769
6-n	8041	25755	0	31740	1.000000	0.202132	0.515686	0.300907
6-m	38173	1358	24397	1608	0.610085	0.959579	0.603195	0.028915
6-d	37815	25503	252	1966	0.993380	0.950579	0.966156	0.931253
7-n	3213	47332	19	14972	0.994121	0.176684	0.771255	0.364534
7-m	17876	43120	4231	309	0.808613	0.983008	0.930725	0.846322
7-d	14740	46846	505	3445	0.966874	0.810558	0.939728	0.847704
8-n	4494	22158	0	38884	1.000000	0.103601	0.406677	0.193924
8-m	42118	133	22025	1260	0.656627	0.970953	0.644699	-0.075582
8-d	24348	22141	17	19030	0.999302	0.561298	0.709366	0.548682
9-n	4890	53207	3	7436	0.999387	0.396722	0.886490	0.589732
9-m	12325	49186	4024	1	0.753869	0.999919	0.938583	0.834732
9-d	12298	52633	577	28	0.955184	0.997728	0.990768	0.970635
10-n	14187	31146	2	20201	0.999859	0.412557	0.691727	0.500151
10-m	34387	30887	261	1	0.992467	0.999971	0.996002	0.992013
10-d	34384	31013	135	4	0.996089	0.999884	0.997879	0.995755
11-n	14671	40720	132	10013	0.991083	0.594353	0.845200	0.684969
11-m	24500	3572	37280	184	0.396568	0.992546	0.428345	0.166735
11-d	24030	35179	5673	654	0.809009	0.973505	0.903458	0.812402
12-n	7204	45666	295	12371	0.960661	0.368020	0.806732	0.519903
12-m	19530	776	45185	45	0.301785	0.997701	0.309845	0.060018
12-d	19408	39947	6014	167	0.763433	0.991469	0.905685	0.808358

13-n	2608	53651	1298	7979	0.667691	0.246340	0.858444	0.346226
13-m	10541	2533	52416	46	0.167432	0.995655	0.199493	0.079031
13-d	10320	44499	10450	267	0.496870	0.974780	0.836472	0.620618
14-n	1461	51387	508	12180	0.742001	0.107104	0.806396	0.231433
14-m	13641	0	51895	0	0.208145	1.000000	0.208145	NaN
14-d	10154	47865	4030	3487	0.715877	0.744374	0.885300	0.657278
15-n	936	62133	33	2434	0.965944	0.277745	0.962357	0.507270
15-m	3370	3061	59105	0	0.053942	1.000000	0.098129	0.051537
15-d	3363	61528	638	7	0.840540	0.997923	0.990158	0.911074
16-n	4543	58089	4	2900	0.999120	0.610372	0.955688	0.762067
16-m	7443	99	57994	0	0.113743	1.000000	0.115082	0.013923
16-d	7437	56680	1413	6	0.840339	0.999194	0.978348	0.905052
17-n	2858	55353	634	6691	0.818442	0.299298	0.888229	0.452365
17-m	9536	298	55689	13	0.146202	0.998639	0.150055	0.020336
17-d	9006	50960	5027	543	0.641773	0.943135	0.915009	0.733933
18-n	10662	28372	3	26499	0.999719	0.286914	0.595612	0.384991
18-m	37161	0	28375	0	0.567032	1.000000	0.567032	NaN
18-d	34845	28118	257	2316	0.992678	0.937677	0.960739	0.922580
19-n	6080	49795	190	9471	0.969697	0.390972	0.852585	0.559970
19-m	15551	21811	28174	0	0.355655	1.000000	0.570099	0.393942
19-d	15144	48771	1214	407	0.925786	0.973828	0.975266	0.933388
20-n	7631	52325	94	5486	0.987832	0.581764	0.914856	0.719637
20-m	13112	31433	20986	5	0.384539	0.999619	0.679703	0.479944
20-d	12993	50360	2059	124	0.863208	0.990547	0.966690	0.904878
21-n	5859	54029	0	5648	1.000000	0.509168	0.913818	0.678954
21-m	11504	410	53619	3	0.176650	0.999739	0.181793	0.035231
21-d	9386	54016	13	2121	0.998617	0.815677	0.967438	0.885155
22-n	9992	36090	0	19454	1.000000	0.339333	0.703156	0.469557
22-m	29446	0	36090	0	0.449310	1.000000	0.449310	NaN
22-d	29163	35176	914	283	0.969611	0.990389	0.981735	0.963345
23-n	11850	49497	42	4147	0.996468	0.740764	0.936081	0.824684
23-m	15994	48127	1412	3	0.918879	0.999812	0.978409	0.944698
23-d	15978	48665	874	19	0.948137	0.998812	0.986374	0.964313
24-n	3284	57098	577	4577	0.850557	0.417759	0.921356	0.562635
24-m	7861	1055	56620	0	0.121912	1.000000	0.136047	0.047223
24-d	7844	50004	7671	17	0.505575	0.997837	0.882690	0.661018
25-n	5597	32002	27	27910	0.995199	0.167040	0.573715	0.296608

25-m	33507	0	32029	0	0.511276	1.000000	0.511276	NaN
25-d	31767	31142	887	1740	0.972836	0.948071	0.959915	0.920148

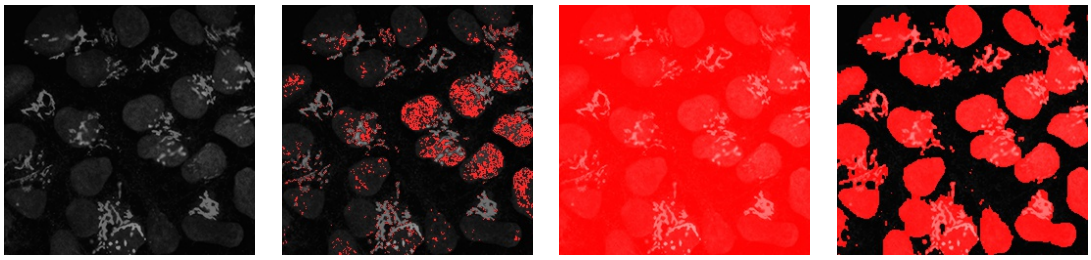

(a) Original. (b) El-Zehiry *et al*. (c) Masaka *et al*. (d) Proposed. $\lambda_1 = 118.726$.

Fig. 31. Image 25 from test set segmentation results.

VI. Conclusion

Lorem ipsum dolor sit amet, consectetuer adipiscing elit. Etiam lobortis facilisis sem. Nullam nec mi et neque pharetra sollicitudin. Praesent imperdiet mi nec ante. Donec ullamcorper, felis non sodales commodo, lectus velit ultrices augue, a dignissim nibh lectus placerat pede. Vivamus nunc nunc, molestie ut, ultricies vel, semper in, velit. Ut porttitor. Praesent in sapien. Lorem ipsum dolor sit amet, consectetuer adipiscing elit. Duis fringilla tristique neque. Sed interdum libero ut metus. Pellentesque placerat. Nam rutrum augue a leo. Morbi sed elit sit amet ante lobortis sollicitudin. Praesent blandit blandit mauris. Praesent lectus tellus, aliquet aliquam, luctus a, egestas a, turpis. Mauris lacinia lorem sit amet ipsum. Nunc quis urna dictum turpis accumsan semper.

Acknowledgment

The authors would like to thank...

References

[1] H. Kopka and P. W. Daly, *A Guide to LaTeX*, 3rd ed. Harlow, England: Addison-Wesley, 1999.